Advances in Continuous
and Discrete Models

RESEARCH Open Access

Numerical analysis of time-fractional Sobolev equation for fluid-driven processes in impermeable rocks

Zakieh Avazzadeh[1], Omid Nikan[2*], José Tenreiro Machado[3] and Mohammad Navaz Rasoulizadeh[4]

*Correspondence:
omidnikan77@yahoo.com
[2]School of Mathematics, Iran University of Science and Technology, Narmak, Tehran, Iran
Full list of author information is available at the end of the article

Abstract

This paper proposes a local meshless radial basis function (RBF) method to obtain the solution of the two-dimensional time-fractional Sobolev equation. The model is formulated with the Caputo fractional derivative. The method uses the RBF to approximate the spatial operator, and a finite-difference algorithm as the time-stepping approach for the solution in time. The stability of the technique is examined by using the matrix method. Finally, two numerical examples are given to verify the numerical performance and efficiency of the method.

Keywords: Local meshless method; RBF; Finite difference; Caputo fractional derivative; Time-fractional Sobolev equation; Stability

1 Introduction

Extending integer derivatives to fractional orders in differential equations led to an area in mathematics called fractional calculus (FC) [1–4]. This field, dealing with the calculus of derivatives and integrals of arbitrary order, became popular in the last thirty years, since numerous significant phenomena in signal processing and optics [5–7], biological systems [8], quantum mechanics [9], electrochemistry [10], fluid mechanics [11], viscoelasticity [12], and electromagnetics [13] can be described via fractional differential equations (FDEs). Moreover, FC is presently a key tool in the modeling of particle transport occurring in porous heterogeneous media in addition to complex phenomena [1, 2]. Therefore, researchers need an effective tool to solve FDEs; however, obtaining exact solutions for such equations is difficult. Hence, it is becoming increasingly important to develop efficient numerical techniques to tackle these problems [14]. Nevertheless, numerical schemes for FDEs lead to mathematical difficulties not faced in integer-order model analysis. The main reasons for this are that the fractional difference operators have a nonlocal nature and their adjoints are not the negatives of themselves [15].

From the perspective of the numerical analysis, there are some fundamental difficulties in numerically solving the fractional derivatives, because some of the good properties of classical approximating operators are lost. During the last decades, the difference method has made some developments for approximating FDEs, [16, 17]. The Riemann–Liouville fractional derivative can be discretized by the standard Grünwald–Letnikov formula [18] with only first-order accuracy, but the difference scheme based on the Grünwal–Letnikov formula for time-dependent problems is unstable [16]. To tackle this problem, Meerschaert and Tadjeran [16] presented the shifted Grünwald–Letnikov formula to simulate fractional advection–dispersion flow equations. Sousaa and Li [19] adopted a second-order discretization for the Riemann–Liouville fractional derivative and established an unconditionally stable weighted average difference method. Ortigueira [20] advanced the fractional centred derivative to solve the Riesz fractional derivative with second-order accuracy. It is worth mentioning that the singularity of the exact solution for time FDEs often occurs near the starting time $t = 0$ [21]. Therefore, one needs to establish some proper regularity assumptions to develop the numerical schemes [21]. As a result, constructing fast and high-order numerical techniques to solve FDEs is a challenging task.

Hereafter, we study a numerical approach to solve the time-fractional Sobolev equation (TFSE) as

$$\frac{\partial^\alpha u(\mathbf{x},t)}{\partial t^\alpha} - \gamma \frac{\partial \nabla^2 u(\mathbf{x},t)}{\partial t} - \sigma \nabla^2 u(\mathbf{x},t) = f(\mathbf{x},t), \quad 0 < t \leq T, \mathbf{x} = (x,y) \in \Omega \subset \mathbb{R}^2, \tag{1}$$

with the initial condition (IC)

$$u(\mathbf{x},0) = g(\mathbf{x}), \quad \mathbf{x} \in \Omega, \tag{2}$$

and the boundary condition (BC)

$$u(\mathbf{x},t) = h(\mathbf{x},t), \quad \mathbf{x} \in \partial\Omega, 0 \leq t \leq T, \tag{3}$$

where γ and σ denote two positive constants, Ω expresses a continuous domain in $\mathbb{R}^2$ with boundary $\partial\Omega$, ∇^2 represents a Laplacian operator in the variable space, T stands for the total time, and $u(\mathbf{x},t)$ is the unknown solution to be determined. The time-fractional derivative in the TFSE denotes the Caputo fractional derivative of order α expressed by

$$\frac{\partial^\alpha u(\mathbf{x},t)}{\partial t^\alpha} = \begin{cases} \frac{1}{\Gamma(1-\alpha)} \int_0^t \frac{\partial u(\mathbf{x},\eta)}{\partial \eta} \frac{1}{(t-\eta)^\alpha} \, \mathrm{d}\eta, & 0 < \alpha < 1, \\ \frac{\partial u(\mathbf{x},t)}{\partial t}, & \alpha = 1. \end{cases} \tag{4}$$

Here, the process of modeling fluids is developed using the fractional derivative operator. This generalization includes by means of the Caputo fractional derivative instead of the standard temporal derivative. When $\alpha = 1$, the TFSE yields the classical pseudoparabolic or Sobolev equation that describes various fluid-mechanics and engineering problems, e.g., quasistationary phenomena in semiconductors, thermal conduction with conductive or thermodynamic temperature, and the flow of fluid through fissured rocks [22]. Indeed, the Sobolev equation is the mathematical model of the vertical nonstationary groundwater flow with dynamic capillary-pressure effect in a porous medium (see [23] and references therein). A noteworthy characteristic of these models consists of their capability of expressing the conservation of some quantities, such as mass, heat, and momentum [22]. The Sobolev model is a special class of the Benjamin–Bona–Mahony–Burgers (BBMB) equation, where the coefficients of the nonlinear term and first-order derivatives equal zero [24].

Some numerical techniques have been advanced to approximate the TFSE. Liu et al. [25] applied a modified reduced-order finite-element (FE) technique. Haq and Hussain [26, 27] developed a meshless scheme based on radial basis functions (RBFs). Beshtokov [28] proposed a finite-difference algorithm, while Qin et al. [29] employed a Newton linearized scheme based on the Crank–Nicolson technique and Zhao et al. [30] used a finite-volume element (FVE) approach.

We find in the technical literature three standard numerical approaches, namely the finite element, the finite difference, and the finite volume (abbreviated, FE, FD, and FV) schemes. These approaches have been successfully used to approximate a variety of partial differential equations (PDEs) in diverse subject areas, such as electromagnetism, fluid dynamics, material science, financial markets, and astrophysics. In fact, the behavior of some materials in nature may be modeled via PDEs and solved by traditional numerical methods. Examples include climate and weather modeling performed in geophysics, Navier–Stokes equations arising in fluid dynamics, biphasic modeling in engineering, and Maxwell's equations used in electrodynamics. The FD is common in science and engineering for its simplicity. However, the main shortcoming of the FD is its inability to handle higher-dimensional geometries since the PDE discretization depends on a topological line grid. On the other hand, the FE is the most flexible traditional method with respect to geometry. An alternative strategy is the so-called spectral method. This is an accurate method, but it suffers from geometric restrictions and has predetermined periodic boundary conditions in the Fourier case. The computational domain in the FE is partitioned into smaller subdomains and the solution is constructed in each element using the basis functions. Consequently, the number of dimensions or variables may reach hundreds or thousands in a real-world problem. Hence, the question arises as to whether it is possible to generate grid points in problems with irregular domains and complex geometries in higher dimensions. This problem led to the development of meshless (or mesh-free) methods that are meshless in the sense that they do not require point connectivity in the mesh/grid. Determining the nearest neighbors involves a smaller computational cost than mesh generation in traditional methods.

The RBFs are gaining popularity in the interpolation of functions and the solution of partial differential equations (PDEs) owing to their simplicity and accuracy [31–33]. In addition, RBF techniques reveal almost spectral accuracy [34, 35] and are easy to implement since they are independent of the node location and the problem dimension. Nonetheless, global RBF (GRBF) approximations result in ill-conditioned and full matrices, which makes them unsuitable for large problems. Consequently, local strategies, such as the RBF partition of unity (RBF-PU) [23, 36–41] and the RBF-generated finite-difference (RBF-FD) approaches [42–45], are currently under development.

The main idea behind the RBF-PU is to decompose the original domain into several covering subdomains (patches) and to construct a local RBF approximant over each subdomain. The localized method overcomes the large computational cost posed by the ill-conditioned and dense matrices of the GRBF method, while maintaining the accuracy resulting from the sparsity of such matrices. Moreover, the RBF-PU also achieves good accuracy with significantly less computational burden than the GRBF.

This paper is outlined as follows. Section 2 provides a time-discrete scheme using the finite-difference (FD) formula through the θ-weighted rule. Section 3 discusses the spatial discretization using the RBF-PU. In addition, the stability of the RBF-PU collocation through the matrix method is also analyzed. Section 4 presents two numerical problems that exemplify the accuracy and efficiency of the RBF-PU. Finally, Sect. 5 highlights the main conclusions.

2 Discretization of the time derivative

This section constructs the semitime-discrete algorithm using a FD formula with a θ-weighted scheme. For this purpose, let $0 = t_0 < t_1 < \cdots < t_L = T$ denote the time instants for the interval $[0, T]$ so that L and $\delta t = T/L$ are the positive integer the time step, respectively. The terms $\frac{\partial u(\mathbf{x},t)}{\partial t}$ and $\frac{\partial \Delta u(\mathbf{x},t)}{\partial t}$ can be approximated at the nodal point t_{n+1} as

$$\frac{\partial u(\mathbf{x}, t_{n+1})}{\partial t} = \frac{u(\mathbf{x}, t_{n+1}) - u(\mathbf{x}, t_n)}{\delta t} + \mathcal{O}(\delta t), \tag{5}$$

$$\frac{\partial \Delta u(\mathbf{x}, t_{n+1})}{\partial t} = \frac{\Delta u(\mathbf{x}, t_{n+1}) - \Delta u(\mathbf{x}, t_n)}{\delta t} + \mathcal{O}(\delta t). \tag{6}$$

Moreover, the Caputo-time-fractional derivative of $u(\mathbf{x}, t)$ appearing in Eq. (1) can be approximated as

$$\begin{aligned}
&\frac{\partial^\alpha u(\mathbf{x}, t_{n+1})}{\partial t^\alpha} \\
&= \frac{1}{\Gamma(1-\alpha)} \int_0^{t_{n+1}} \frac{\partial u(\mathbf{x}, \eta)}{\partial \eta} \frac{1}{(t_{n+1} - \eta)^\alpha} \, \mathrm{d}\eta \\
&= \frac{1}{\Gamma(1-\alpha)} \sum_{k=0}^{n} \int_{k\delta t}^{(k+1)\delta t} \frac{\partial u(\mathbf{x}, \eta_{k+1})}{\partial \eta} \frac{1}{(t_{n+1} - \eta)^\alpha} \, \mathrm{d}\eta \\
&\approx \frac{1}{\Gamma(1-\alpha)} \sum_{k=0}^{n} \int_{k\delta t}^{(k+1)\delta t} \frac{\partial u(\mathbf{x}, \eta_{k+1})}{\partial \eta} \frac{1}{(t_{n+1} - \eta)^\alpha} \, \mathrm{d}\eta \\
&= \frac{1}{\Gamma(1-\alpha)} \sum_{k=0}^{n} \left(\frac{u(\mathbf{x}, t_{k+1}) - u(\mathbf{x}, t_k)}{\delta t} + \mathcal{O}(\delta t) \right) \int_{k\delta t}^{(k+1)\delta t} \frac{1}{(t - \eta)^\alpha} \, \mathrm{d}\eta \\
&= \frac{1}{\Gamma(1-\alpha)} \sum_{k=0}^{n} \left(\frac{u(\mathbf{x}, t_{k+1}) - u(\mathbf{x}, t_k)}{\delta t} + \mathcal{O}(\delta t) \right) \int_{k\delta t}^{(k+1)\delta t} \frac{\mathrm{d}r}{r^\alpha} \\
&= \begin{cases} \frac{\delta t^{-\alpha}}{\Gamma(2-\alpha)} (u^{n+1} - u^n) + \frac{\delta t^{-\alpha}}{\Gamma(2-\alpha)} \sum_{k=1}^{n} [(k+1)^{1-\alpha} - k^{1-\alpha}](u^{n+1-k} - u^{n-k}), & n \geq 1, \\ \frac{\delta t^{-\alpha}}{\Gamma(2-\alpha)} (u^1 - u^0), & n = 0 \end{cases} \\
&= \begin{cases} a_0 [(u^{n+1} - u^n) + \sum_{k=1}^{n} b_k (u^{n+1-k} - u^{n-k})], & n \geq 1, \\ a_0 (u^1 - u^0), & n = 0 \end{cases} + \mathcal{O}\bigl(\delta t^{2-\alpha}\bigr),
\end{aligned} \tag{7}$$

where $u(x, t_{n+1}) = u^{n+1}$, $a_0 = \frac{\delta t^{-\alpha}}{\Gamma(2-\alpha)}$ and $b_k = (k+1)^{1-\alpha} - k^{1-\alpha}$.

Inserting Eqs. (6) and (7) into Eq. (1) together with the θ-weighted formula gives the semitime-discrete approach between successive two temporal levels n and $n+1$:

$$\begin{aligned}
&a_\alpha u^{n+1} - r_\theta \nabla^2 u^{n+1} \\
&= \begin{cases} a_\alpha u^n - s_\theta \nabla^2 u^n - a_\alpha \sum_{j=1}^{n} b_j (u^{n+1-j} - u^{n-j}) + \delta t f_\theta^{n+1}, & n \geq 1, \\ a_\alpha u^0 - s_\theta \nabla^2 u^0 + \delta t f_\theta^1, & n = 0, \end{cases}
\end{aligned} \tag{8}$$

where $a_\alpha = a_0 \delta t$, $r_\theta = \sigma \theta \delta t + \gamma$, $s_\theta = \sigma(1-\theta)\delta t + \gamma$ and $f_\theta^{n+1} = (1-\theta) f^n + \theta f^{n+1}$.

3 Spatial derivative discretization

This section describes the LRBF-PU collocation scheme. The PU technique determines the numerical solution via a weighted sum of the local approximants created on overlapping subdomains. The RBFs are applied as local approximants and Wendland's compactly supported RBFs [46] are adopted as weight functions. This strategy is based on constructing differentiation matrices that convert a given PDE into an algebraic system. The benefit of RBF-PU comes from its low computational cost owing to its relatively sparse matrices.

Let $\Xi = \{\mathbf{x}_1, \dots, \mathbf{x}_N\} \subseteq \mathbb{R}^d$, be a set of scattered data sites, the RBF interpolant $S(\mathbf{x})$ of $u(\mathbf{x})$ to the data points $u_j = u(\mathbf{x}_j)$, $j = 1, \dots, N$, takes the following form:

$$u(\mathbf{x}) \simeq S(\mathbf{x}) = \sum_{j=1}^{N} a_j \phi_j(\mathbf{x}, \varepsilon), \tag{9}$$

in which a_j represent the coefficients to be determined from the data, $\phi_j(\mathbf{x}, \varepsilon) = \phi(\|\mathbf{x} - \mathbf{x}_j\|_2, \varepsilon)$, $j = 1, \dots, N$, are the RBFs, $r = \|\mathbf{x} - \mathbf{x}_j\|_2$ stands for the Euclidean norm and $\mathbf{x}_j$ are centers coinciding with the collocation points. The constant ε denotes the shape parameter, which is responsible for the flatness of the functions. To compute the unknown coefficients λ_j, we can impose the interpolation conditions $S(\mathbf{x}_i) = u_i$, $i = 1, \dots, N$) and as a result we obtain a $N \times N$ linear system

$$A\lambda = u, \tag{10}$$

in which $\lambda = [a_1, \dots, a_N]^{\mathrm{T}}$, $u = [u(\mathbf{x}_1), \dots, u(\mathbf{x}_N)]^{\mathrm{T}}$, and the entries of A are $A_{ij} = \phi(\|\mathbf{x}_i - \mathbf{x}_j\|_2, \varepsilon)$ (the symbol T means transpose).

We can construct the Lagrange basis $\psi_1(\mathbf{x}), \dots, \psi_N(\mathbf{x})$ of the span of the functions ϕ_j as

$$S(\mathbf{x}) = \sum_{j=1}^{N} \psi_j(\mathbf{x}) u(\mathbf{x}). \tag{11}$$

Thus, the alternative expression for the interpolant (9) can be illustrated as:

$$S(\mathbf{x}) = \Psi(\mathbf{x}) u, \tag{12}$$

in which $\Psi(\mathbf{x}) = [\psi_1(\mathbf{x}), \dots, \psi_N(\mathbf{x})]^{\mathrm{T}}$.

In view of Eqs. (12), (10), and (9), we deduce the relation between the original basis and the Lagrange radial basis as

$$\Psi(\mathbf{x}) = \Phi A^{-1}, \tag{13}$$

in which $\Phi = [\phi(\|\mathbf{x} - \mathbf{x}_1\|_2, \varepsilon), \dots, \phi(\|\mathbf{x} - \mathbf{x}_N\|_2, \varepsilon)]^{\mathrm{T}}$.

The nonsingularity of matrix A guarantees that the transformation (13) is valid.

Let $\Omega \subset \mathbb{R}^2$ be an open and bounded domain, and $\Xi = \{\mathbf{x}_1, \dots, \mathbf{x}_N\} \subseteq \mathbb{R}^d$ a set of collocation nodes. We partition $\Omega \subset \mathbb{R}^2$ into M patches or subdomains $\{\Omega_j\}_{j=1}^{M}$ of the domain Ω so that $\Omega \subset \bigcup_{j=1}^{M} \Omega_j$. Figure 1 represents a schematic diagram of the square domain Ω along with the related circular subdomains. Also, we define

$$I(\mathbf{x}) = \{j : \mathbf{x} \in \Omega_j\}, \qquad \operatorname{card}(I)(\mathbf{x}) \le C,$$

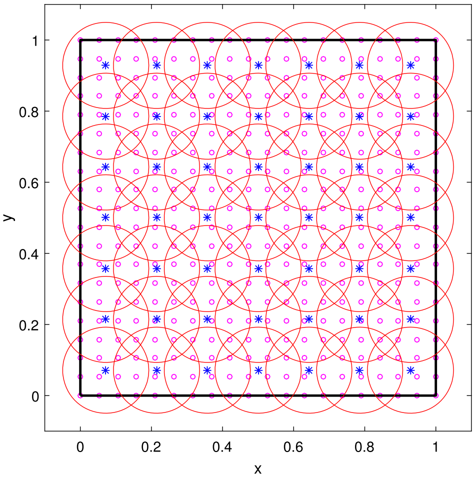

Figure 1 Illustration diagram of computational domain with circular subdomains

in which the constant C is independent of the number of subdomains [46]. The PU weight functions w_j can be established based on Shepard's method [47] as follows:

$$w_j(\mathbf{x}) = \frac{\varphi_j(\mathbf{x})}{\sum_{k\in I(\mathbf{x})} \varphi_k(\mathbf{x})}, \tag{14}$$

in which $\varphi_j(\mathbf{x})$ is a compactly supported function on each subdomain Ω_j. It follows that $w_j(\mathbf{x}) = 0\ \forall j \notin I(\mathbf{x})$. To ensure the nonnegativity and compact support in subdomain Ω_j, we consider in (14)

$$\varphi_j(\mathbf{x}) = \varphi_j\left(\frac{\|\mathbf{x} - \tilde{\mathbf{x}}_j\|}{\rho_j}\right), \quad j = 1, 2, \ldots, M. \tag{15}$$

Here, ρ_j denotes the radius of the subdomain Ω_j and $\tilde{\mathbf{x}}_j$ represents its center node. The function φ_j denotes one of the compact functions with minimal degree [48]. Hereafter, we adopt the Wendland function $\varphi(r) = (1 + 4r)_+(1 - r)^4$, where $r = \frac{\|\mathbf{x}-\tilde{\mathbf{x}}_j\|}{\rho_j}$ [46].

The global approximant is thus constructed in the computational domain Ω as follows

$$\mathcal{P}_u(\mathbf{x}) = \sum_{j\in I(\mathbf{x})} w_j(\mathbf{x}) S_j(\mathbf{x}) = \sum_{j\in I(\mathbf{x})} \sum_{i\in J(\Omega_j)} w_j(\mathbf{x}) \psi_i(\mathbf{x}) u(\mathbf{x}), \tag{16}$$

where $\{S_j\}_{j=1}^k$ defines a local RBF interpolant on each subdomain Ω_j.

We approximate a spatial differential operator $\frac{\partial^{|\sigma|}}{\partial \mathbf{x}^\sigma}$ at the interior nodes in order to use the LRBF-PU for the spatial discretization of the PDE as

$$\begin{aligned} \frac{\partial^{|\sigma|}}{\partial \mathbf{x}^\sigma} \mathcal{P}_u(\mathbf{x}) &= \sum_{j\in I(\mathbf{x})} \sum_{i\in J(\Omega_j)} \frac{\partial^{|\sigma|}}{\partial \mathbf{x}^\sigma} \big(w_j(\mathbf{x}) \psi_i(\mathbf{x})\big) u(\mathbf{x}_i) \\ &= \sum_{j\in I(\mathbf{x})} \sum_{i\in J(\Omega_j)} \left[\sum_{\boldsymbol{\vartheta} \le \boldsymbol{\sigma}} \binom{\boldsymbol{\sigma}}{\boldsymbol{\vartheta}} \frac{\partial^{|\sigma-\vartheta|} w_j}{\partial \mathbf{x}^{\sigma-\vartheta}}(\mathbf{x}) \frac{\partial^{|\vartheta|} \psi_i}{\partial \mathbf{x}^{\vartheta}}(\mathbf{x}) \right] u(\mathbf{x}_i), \end{aligned} \tag{17}$$

where $\boldsymbol{\sigma}$ and $\boldsymbol{\vartheta} \in \mathbb{N}_0^d$. The evaluation of the Laplace operator can be represented as

$$\nabla^2 v(\mathbf{x}) = \sum_{j\in I(\mathbf{x})} \sum_{i\in J(\Omega_j)} \left[\psi_j(\mathbf{x})\nabla^2 w_j(\mathbf{x}) + 2\nabla^2 w_j(\mathbf{x})\nabla^2 \psi_j(\mathbf{x}) + \nabla^2 \psi_j(\mathbf{x}) w_j(\mathbf{x})\right] v(\mathbf{x}_i). \tag{18}$$

From (16), we express the approximation solution V^k by the following expression:

$$U^k \approx \mathcal{P}_u(\mathbf{x}) = \sum_{j\in I(\mathbf{x})} \sum_{i\in J(\Omega_j)} w_j(\mathbf{x})\psi_i(\mathbf{x}) U^k. \tag{19}$$

We divide the collocation points into two sets, $\mathcal{J}$ and $\mathcal{I}$, considered to be sets of boundary and internal points, respectively. Moreover, the overall number of points is equal to N with $N = N_{\mathcal{J}} + N_{\mathcal{I}}$, so that $N = N_{\mathcal{I}}$ and $N = N_{\mathcal{J}}$ denote the total numbers of internal and boundary points, respectively. We split matrix A into 2 matrices, $A_{\mathcal{I}}$ and $A_{\mathcal{J}}$, as follows

$$A = A_{\mathcal{I}} + A_{\mathcal{J}}, \tag{20}$$

in which

$$\begin{aligned}
&A = \left[w_j(\mathbf{x}_i)\psi_i(\mathbf{x}_i) : j \in I(\mathbf{x}_i) \text{ and } 0 \text{ o. w}\right]_{N\times N},\\
&A_{\mathcal{I}} = [A_{ij} : i \in \mathcal{I}, 1 \le j \le N \text{ and } 0 \text{ o. w}]_{N\times N},\\
&A_{\mathcal{J}} = [A_{ij} : i \in \mathcal{J}, 1 \le j \le N \text{ and } 0 \text{ o. w}]_{N\times N}.
\end{aligned}$$

Inserting Eq. (19) into Eq. (8) gives a system of N linear equations in the matrix form

$$\begin{aligned}
&\tilde{\mathbf{A}}\mathbf{U}^1 = \tilde{\mathbf{B}}g + \tilde{\mathbf{H}}, \qquad (21)\\
&\tilde{\mathbf{A}} = a_\alpha A - r_\theta \nabla^2 A_{\mathcal{I}},\\
&\tilde{\mathbf{B}} = a_\alpha A_{\mathcal{I}} - s_\theta A_{\mathcal{I}},\\
&\tilde{\mathbf{H}} = \left[\delta t f_\theta^1 : i \in \mathcal{I} \text{ and } h_j : j \in \mathcal{J}\right]^{\mathrm{T}},\\
&\mathbf{U}^1 = \left[U_1^1, \dots, U_N^1\right]^{\mathrm{T}}.
\end{aligned}$$

When $k \ge 1$, we obtain

$$\mathbf{A}\mathbf{U}^{n+1} = \mathbf{B}\mathbf{U}^n + \mathbf{H}, \tag{22}$$

where

$$\begin{aligned}
&\mathbf{A} = a_\alpha A - r_\theta \nabla^2 A_{\mathcal{I}},\\
&\mathbf{B} = a_\alpha A_{\mathcal{I}} - s_\theta A_{\mathcal{I}},\\
&\mathbf{H} = \left[\delta t f_\theta^{n+1} - a_\alpha \sum_{j=1}^{n} b_j\left(U^{n+1-j} - U^{n-j}\right) : i \in \mathcal{I} \text{ and } h_j : j \in \mathcal{J}\right]^{\mathrm{T}},\\
&\mathbf{U}^{n+1} = \left[U_1^{n+1}, \dots, U_N^{n+1}\right]^{\mathrm{T}}.
\end{aligned}$$

Using system (22), we can calculate the numerical solution at any temporal step n.

3.1 Stability analysis

Here, we investigate the stability of the RBF collocation approximation (22) based on the matrix method. Let us define the error e^n at the nth time level as

$$e^n = u^n - U^n, \tag{23}$$

where u^n and U^n are the analytic and approximate solutions at the nth time level, respectively. Then, the error equation of (22) can be written as

$$\mathbf{e}^{n+1} = A\mathbf{A}^{-1}\mathbf{B}A^{-1}\mathbf{e}^n, \tag{24}$$

where $\mathbf{P} = A\mathbf{A}^{-1}\mathbf{B}A^{-1}$ is called the amplification matrix.

Due to the Lax–Richtmyer definition of stability, Eq. (24) is said to be stable if $\|\mathbf{P}\| \leq 1$, which is equivalent to $\rho(\mathbf{P}) \leq 1$, where $\rho(\mathbf{P})$, represents the spectral radius of the matrix $\mathbf{P}$.

4 Numerical examples

This section illustrates the effectiveness of the RBF-PU by means of two numerical examples on the TFSE. To assess the accuracy, we calculate the error norms L_∞, L_2 and L_{rms} defined as:

$$L_\infty = \max_{1\leq j\leq N-1} \left|u(\mathbf{x}_j, T) - U(\mathbf{x}_j, T)\right|,$$

$$L_2 = \left(\sum_{j=1}^{N} \left(u(\mathbf{x}_j, T) - U(\mathbf{x}_j, T)\right)^2\right)^{\frac{1}{2}},$$

$$L_{\text{rms}} = \left(\frac{1}{N}\sum_{j=1}^{N} \left(u(\mathbf{x}_j, T) - U(\mathbf{x}_j, T)\right)^2\right)^{\frac{1}{2}},$$

in which u^n and U^n are the analytic and approximated solutions, respectively.

In what follows, $\mathbf{E}_{a,b} = \sum_{k=0}^{\infty} \frac{z^k}{\Gamma(ak+b)}$ is the Mittag–Leffler function of two parameters $a, b \in \mathbb{R}^+$.

Example 1 We consider the 2-dim TFSE as

$$\frac{\partial^\alpha u(\mathbf{x}, t)}{\partial t^\alpha} - \frac{\partial \Delta u(\mathbf{x}, t)}{\partial t} - \Delta u(\mathbf{x}, t) = -t^{1-\alpha}\mathbf{E}_{1,2-\alpha} \sin(\pi x)\sin(\pi y), \quad \Omega = [0,1]^2.$$

The IC and BC can be determined from the exact solution $u(x, y, t) = \exp(-t)\sin(\pi x) \times \sin(\pi y)$.

Table 1 presents the numerical errors L_∞, L_2, and L_{rms} and the associated condition number $\kappa(\mathbf{A})$ when $N = 225$, $M = 25$ and $T = 1$ at various time steps. Table 2 compares the error norms of the LRBF-PU versus the technique described in [26] at different total times when $\alpha = 0.5$. We can see that the computational accuracy of the RBF-PU is close to [26]. Table 3 presents the values of L_∞, $\kappa(\mathbf{A})$ and the CPU running time (in seconds) for a time-step size $\delta t = 1/200$ at $T = 1$. Figure 2 depicts the sparsity structure of the matrix $\mathbf{A}$

Table 1 Error norms and associated condition number $\kappa(\mathbf{A})$ of Example 1 when $N = 225$, $M = 25$ and $T = 1$ at various time steps

δt	L_∞	L_2	L_{rms}	$\kappa(\mathbf{A})$
1/5	1.2615e–03	2.2800e–03	5.8869e–04	8.2114e+04
1/10	3.1440e–04	5.6825e–04	1.4672e–04	7.8243e+04
1/20	7.8540e–05	1.4195e–04	3.6652e–05	7.6307e+04
1/40	1.9631e–05	3.5481e–05	9.1613e–06	7.5340e+04
1/80	4.9076e–06	8.8699e–06	2.2902e–06	7.4856e+04
1/160	1.2269e–06	2.2175e–06	5.7254e–07	7.4614e+04
1/320	3.0672e–07	5.5436e–07	1.4314e–07	7.4493e+04
1/640	7.6680e–08	1.3859e–07	3.5784e–08	7.4433e+04
1/1280	1.9170e–08	3.4647e–08	8.9457e–09	7.4402e+04
1/2560	4.7868e–09	8.6517e–09	2.2339e–09	7.4387e+04
1/5120	1.2030e–09	2.1718e–09	5.6076e–10	7.4380e+04

Table 2 The error norms of LRBF-PU with the technique presented in [26] for Example 1 at various final times when $\alpha = 0.5$

T	Ref. [26]			RBF-PU		
	L_∞	L_2	L_{rms}	L_∞	L_2	L_{rms}
0.1	7.547e–07	3.774e–07	3.659e–07	7.5392e–07	2.0711e–06	3.6612e–07
0.5	2.529e–06	1.265e–06	1.226e–06	1.7717e–06	4.8668e–06	8.6034e–07
1.0	3.068e–06	1.534e–06	1.488e–06	2.1754e–06	5.9760e–06	1.0564e–06
2.0	2.258e–06	1.129e–06	1.095e–06	1.6402e–06	4.5056e–06	7.9649e–07
2.5	1.712e–06	8.559e–07	8.299e–07	1.2589e–06	3.4582e–06	6.1133e–07
3.0	1.246e–06	6.229e–07	6.041e–07	9.2761e–07	2.5482e–06	4.5046e–07
3.5	8.815e–07	4.408e–07	4.274e–07	6.6456e–07	1.8256e–06	3.2272e–07
4.0	6.111e–07	3.055e–07	2.963e–07	4.6642e–07	1.2813e–06	2.2650e–07
4.5	4.170e–07	2.085e–07	2.022e–07	3.2225e–07	8.8524e–07	1.5649e–07
5.0	2.810e–07	1.405e–07	1.362e–07	2.1991e–07	6.0410e–07	1.0679e–07

Table 3 The absolute errors L_∞, associated condition number $\kappa(\mathbf{A})$, and CPU running time of Example 1 when $\delta t = 1/200$

N	M	L_∞	CN	CPU
169	36	8.0906e–07	1.9479e+04	0.673644
324	64	7.7800e–07	9.0369e+04	0.939799
676	81	7.8157e–07	1.6171e+05	1.993186
900	121	7.8455e–07	9.1217e+05	3.179997

for two subdomains, namely $M = 81$ and $M = 49$ with $N = 400$. Figure 3 shows the absolute errors L_∞ at various final times $T \in \{0.1, .5, 1, 2\}$ when $\alpha = 0.5$.

Example 2 We consider the 2-dim TFSE

$$\frac{\partial^\alpha u(\mathbf{x},t)}{\partial t^\alpha} - \frac{\partial \Delta u(\mathbf{x},t)}{\partial t} - \Delta u(\mathbf{x},t) = -t^{1-\alpha}\mathbf{E}_{1,2-\alpha}\exp(x-y)\sin(\pi x)\sin(\pi y), \qquad \Omega = [0,1]^2.$$

The IC and BC can be computed from the exact solution $u(x,y,t) = \exp(x-y-t)\sin(\pi x) \times \sin(\pi y)$.

Table 4 reports the error norms L_∞, L_2, and L_{rms} and the associated condition number $\kappa(\mathbf{A})$ when $N = 225$, $M = 25$ and $T = 1$ at various time steps. Table 5 compares the error norms of the LRBF-PU with the technique described in [26] at different total times when $\alpha = 0.9$. We can conclude from Table 5 that the accuracy of the proposed method is slightly

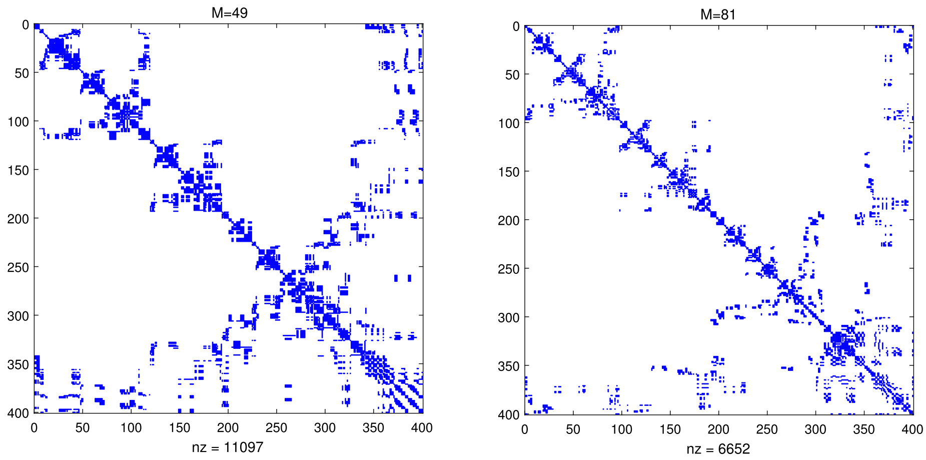

Figure 2 Sparsity structure of the matrix **A** for two subdomains when $N = 400$

Table 4 Error norms and associated condition number $\kappa(\mathbf{A})$ of Example 2 when $N = 225$, $M = 25$ and $T = 1$ at various time steps

δt	L_∞	L_2	L_{rms}	$\kappa(\mathbf{A})$
1/5	1.3814e–03	2.4306e–03	6.2759e–04	9.2470e+04
1/10	3.4428e–04	6.0579e–04	1.5641e–04	8.8109e+04
1/20	8.6003e–05	1.5133e–04	2.1317e–06	8.5929e+04
1/40	2.1497e–05	3.7826e–05	9.7665e–06	8.4839e+04
1/80	5.3739e–06	9.4559e–06	2.4415e–06	8.4294e+04
1/160	1.3435e–06	2.3640e–06	6.1037e–07	8.4022e+04
1/320	3.3586e–07	5.9099e–07	1.5259e–07	8.3885e+04
1/640	8.3968e–08	1.4775e–07	3.8149e–08	8.3817e+04
1/1280	2.0991e–08	3.6936e–08	9.5369e–09	8.3783e+04
1/2560	5.2518e–09	9.2389e–09	2.3855e–09	8.3766e+04
1/5120	1.3134e–09	2.3077e–09	5.9584e–10	8.3758e+04

Table 5 The error norms of LRBF-PU with the technique presented in [26] for Example 2 at various final times when $\alpha = 0.9$

T	Ref. [26]			RBF-PU		
	L_∞	L_2	L_{rms}	L_∞	L_2	L_{rms}
0.1	8.335e–07	4.026e–07	3.904e–07	8.2002e–07	1.1491e–06	3.6336e–07
0.2	1.508e–06	7.286e–07	7.066e–07	1.0500e–06	2.7868e–06	4.9265e–07
0.5	2.794e–06	1.349e–06	1.309e–06	1.9564e–06	5.1939e–06	9.1816e–07
1.0	3.389e–06	1.637e–06	1.587e–06	2.3989e–06	6.3731e–06	1.1266e–06
2.0	2.493e–06	1.204e–06	1.168e–06	1.8057e–06	4.8001e–06	8.4854e–07
3.0	1.376e–06	6.646e–07	6.445e–07	1.0196e–06	2.7123e–06	4.7947e–07
4.0	6.749e–07	3.260e–07	3.161e–07	5.1191e–07	1.3626e–06	2.4087e–07
5.0	3.103e–07	1.499e–07	1.454e–07	2.4099e–07	6.4189e–07	1.1347e–07

superior to that of [26]. Table 6 illustrates the values of L_∞, $\kappa(\mathbf{A})$ and the CPU running time over Ω_1 with a time-step size $\delta t = 1/200$ at $T = 1$. Figure 4 displays the absolute errors L_∞ at various final times $T \in \{0.1, 1, 2, 3, 4, 5\}$ when $\alpha = 0.5$.

5 Conclusions

This work adopted an efficient numerical technique following the RBF-PU collocation technique for finding the solution of the TFSE. A major shortcoming of GRBF colloca-

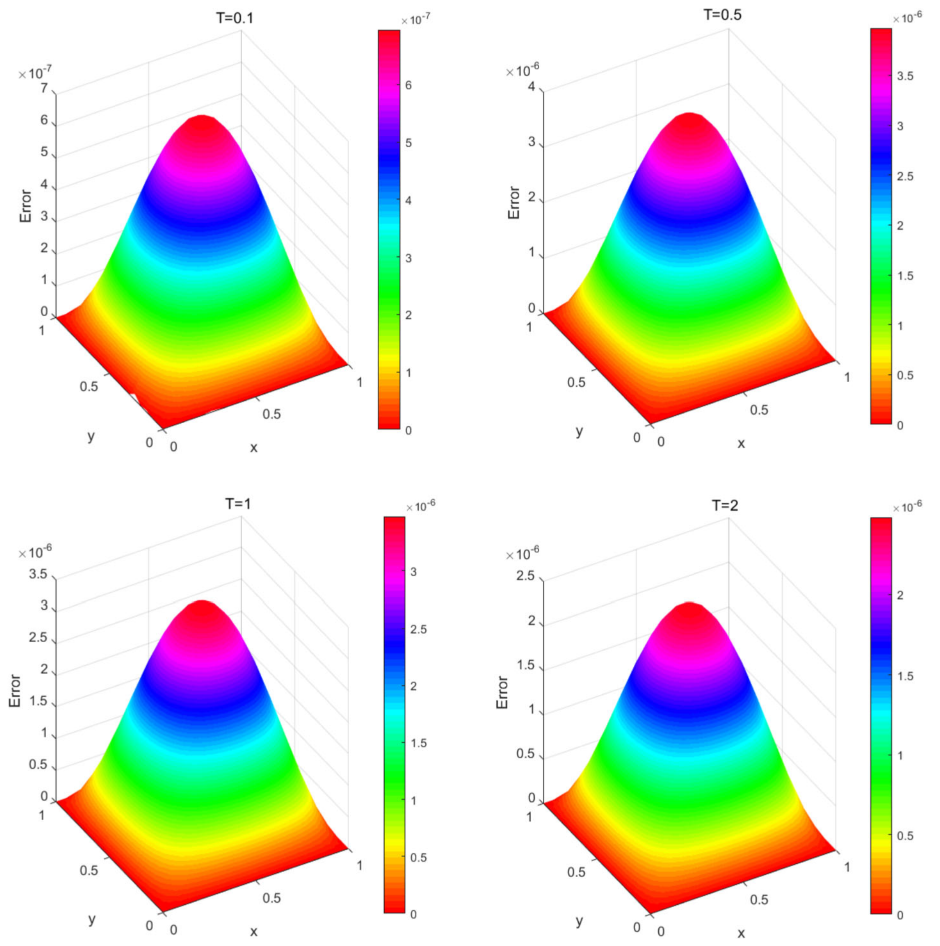

Figure 3 Contour plots of the absolute errors L_∞ for Example 1 at various final times when $\alpha = 0.7$

Table 6 The absolute errors L_∞, associated condition number $\kappa(\mathbf{A})$, and CPU running time of Example 2 when $\delta t = 1/200$

N	M	L_∞	CN	CPU
144	36	8.5808e–07	1.4715e+04	1.205888
324	49	8.6467e–07	1.0882e+05	1.868528
529	64	8.6540e–07	3.7662e+05	1.898207
784	81	8.6558e–07	6.6256e+05	2.735166

tion methods is the computational burden resulting in dense algebraic systems. The local method deals with the ill-conditioning in GRBF schemes and decreases the associated computational time. The proposed strategy consisted of two stages. First, a FD of order $\mathcal{O}(\delta t^{2-\alpha})$, with the θ-rule, $0 \le \theta \le 1$, was implemented to approximate the time dimension. Then, the RBF-PU was provided to discretize the spatial dimension. Numerical experiments illustrated the effectiveness and high accuracy of the RBF-PU.

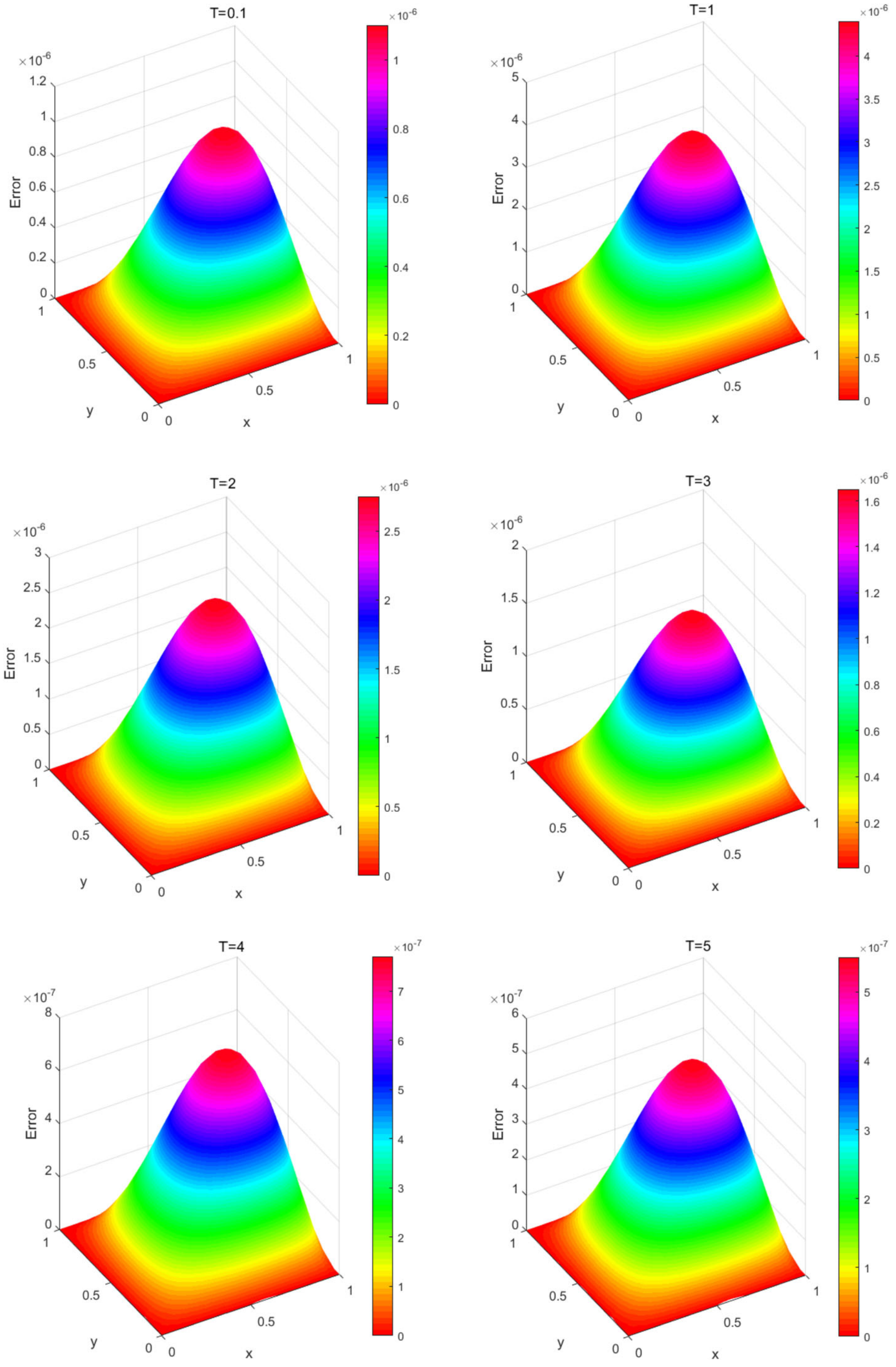

Figure 4 Contour plots of the absolute errors L_∞ for Example 2 at various final times when $\alpha = 0.5$

Acknowledgements
The authors would like to thank the editor and referees for their valuable comments and suggestions that helped us to improve the paper.

Funding
The authors received no financial support for this article.

Availability of data and materials

No datasets were generated or analyzed during the current study.

Declarations

Ethics approval and consent to participate

This article does not contain any studies with human participants or animals performed by any of the authors.

Competing interests

The authors declare that they have no competing interests.

Authors' contributions

All authors contributed equally in writing this manuscript. All authors read and approved the final manuscript.

Author details

[1]Department of Applied Mathematics, Xi'an Jiaotong-Liverpool University, Suzhou, 215123, China. [2]School of Mathematics, Iran University of Science and Technology, Narmak, Tehran, Iran. [3]Institute of Engineering, Polytechnic of Porto, Rua Dr. Antnio B. de Almeida 431, 4249-015 Porto, Portugal. [4]Department of Mathematics, Velayat University, Iranshahr, Iran.

Publisher's Note

Springer Nature remains neutral with regard to jurisdictional claims in published maps and institutional affiliations.

Received: 12 November 2021 Accepted: 17 June 2022 Published online: 28 June 2022

References

1. Oldham, K.B., Spanier, J.: The Fractional Calculus. Mathematics in Science and Engineering., vol. 111. Academic Press, New York (1974)
2. Miller, K.S., Ross, B.: An introduction to the fractional calculus and fractional differential equations (1993)
3. Mainardi, F.: Fractional calculus. In: Some Basic Problems in Continuum and Statistical Mechanics, pp. 291–348. Springer, Vienna (1997)
4. Baleanu, D., Güvenç, Z.B., Machado, J.T., et al.: New Trends in Nanotechnology and Fractional Calculus Applications. Springer, New York (2010)
5. Das, S.: Functional Fractional Calculus. Springer, Berlin (2011)
6. Sabatier, J., Agrawal, O.P., Machado, J.T.: Advances in Fractional Calculus, vol. 4. Springer, Dordrecht (2007)
7. Alieva, T., Bastiaans, M.J., Calvo, M.L.: Fractional transforms in optical information processing. EURASIP J. Adv. Signal Process. **2005**(10), 1–22 (2005)
8. Magin, R.L.: Fractional calculus in bioengineering, part 1. Crit. Rev. Biomed. Eng. **32**(1) (2004)
9. Herrmann, R.: Fractional Calculus: An Introduction for Physicists. World Scientific, GigaHedron (2011)
10. Oldham, K.B.: Fractional differential equations in electrochemistry. Adv. Eng. Softw. **41**(1), 9–12 (2010)
11. Kulish, V.V., Lage, J.L.: Application of fractional calculus to fluid mechanics. J. Fluids Eng. **124**(3), 803–806 (2002)
12. Pipkin, A.C.: Lectures on Viscoelasticity Theory, vol. 7. Springer, New York (2012)
13. Machado, J.T., Jesus, I.S., Galhano, A., Cunha, J.B.: Fractional order electromagnetics. Signal Process. **86**(10), 2637–2644 (2006)
14. Li, C., Zeng, F.: Numerical Methods for Fractional Calculus. Chapman & Hall/CRC, Boca Raton (2019)
15. Wang, H., Yang, D.: Wellposedness of variable-coefficient conservative fractional elliptic differential equations. SIAM J. Numer. Anal. **51**(2), 1088–1107 (2013)
16. Meerschaert, M.M., Tadjeran, C.: Finite difference approximations for fractional advection–dispersion flow equations. J. Comput. Appl. Math. **172**(1), 65–77 (2004)
17. Yang, Q., Liu, F., Turner, I.: Numerical methods for fractional partial differential equations with Riesz space fractional derivatives. Appl. Math. Model. **34**(1), 200–218 (2010)
18. Podlubny, I.: Fractional Differential Equations. Academic Press, San Diego (1999)
19. Sousa, E., Li, C.: A weighted finite difference method for the fractional diffusion equation based on the Riemann–Liouville derivative. Appl. Numer. Math. **90**, 22–37 (2015)
20. Ortigueira, M.D.: Riesz potential operators and inverses via fractional centred derivatives. Int. J. Math. Math. Sci. **2006**, Article ID 048391 (2006)
21. Stynes, M., O'Riordan, E., Gracia, J.L.: Error analysis of a finite difference method on graded meshes for a time-fractional diffusion equation. SIAM J. Numer. Anal. **55**(2), 1057–1079 (2017)
22. Barenblatt, G., Entov, V., Ryzhik, V.: Theory of Fluid Flows Through Natural Rocks. Kluwer Academic, Dordrecht (1990)
23. Nikan, O., Avazzadeh, Z.: A localisation technique based on radial basis function partition of unity for solving Sobolev equation arising in fluid dynamics. Appl. Math. Comput. **401**, 126063 (2021)
24. Dehghan, M., Abbaszadeh, M., Mohebbi, A.: The numerical solution of nonlinear high dimensional generalized Benjamin–Bona–Mahony–Burgers equation via the meshless method of radial basis functions. Comput. Math. Appl. **68**(3), 212–237 (2014)
25. Liu, J., Li, H., Liu, Y.: Crank–Nicolson finite element scheme and modified reduced-order scheme for fractional Sobolev equation. Numer. Funct. Anal. Optim. **39**(15), 1635–1655 (2018)
26. Haq, S., Hussain, M.: Application of meshfree spectral method for the solution of multi-dimensional time-fractional Sobolev equations. Eng. Anal. Bound. Elem. **106**, 201–216 (2019)
27. Hussain, M., Haq, S., Ghafoor, A.: Meshless RBFs method for numerical solutions of two-dimensional high order fractional Sobolev equations. Comput. Math. Appl. **79**(3), 802–816 (2020)

28. Beshtokov, M.K.: Numerical analysis of initial-boundary value problem for a Sobolev-type equation with a fractional-order time derivative. Comput. Math. Math. Phys. **59**(2), 175–192 (2019)
29. Qin, Y., Yang, X., Ren, Y., Xu, Y., Niazi, W.: A Newton linearized Crank-Nicolson method for the nonlinear space fractional Sobolev equation. J. Funct. Spaces **2021**, Article ID 9979791 (2021)
30. Zhao, J., Fang, Z., Li, H., Liu, Y.: A Crank–Nicolson finite volume element method for time fractional Sobolev equations on triangular grids. Mathematics **8**(9), 1591 (2020)
31. Fasshauer, G.E.: Meshfree Approximation Methods with MATLAB, vol. 6. World Scientific, Singapore (2007)
32. Liu, G.-R., Gu, Y.-T.: An Introduction to Meshfree Methods and Their Programming. Springer, Dordrecht (2005)
33. Gu, Y.: Meshfree methods and their comparisons. Int. J. Comput. Methods **2**(4), 477–515 (2005)
34. Madych, W., Nelson, S.: Multivariate interpolation and conditionally positive definite functions. II. Math. Comput. **54**(189), 211–230 (1990)
35. Micchelli, C.A.: Interpolation of scattered data: distance matrices and conditionally positive definite functions. In: Approximation Theory and Spline Functions, pp. 143–145 (1984)
36. Nikan, O., Avazzadeh, Z.: An efficient localized meshless technique for approximating nonlinear sinh-Gordon equation arising in surface theory. Eng. Anal. Bound. Elem. **130**, 268–285 (2021)
37. Nikan, O., Avazzadeh, Z.: Coupling of the Crank–Nicolson scheme and localized meshless technique for viscoelastic wave model in fluid flow. J. Comput. Appl. Math. **1**, 113695 (2021)
38. Nikan, O., Avazzadeh, Z., Machado, J.: Numerical simulation of a degenerate parabolic problem occurring in the spatial diffusion of biological population. Chaos Solitons Fractals **150**, 111169 (2021)
39. Nikan, O., Avazzadeh, Z., Rasoulizadeh, M.: Soliton solutions of the nonlinear sine-Gordon model with Neumann boundary conditions arising in crystal dislocation theory. Nonlinear Dyn. **106**(1), 783–813 (2021)
40. Nikan, O., Avazzadeh, Z., Machado, J.T.: Numerical approach for modeling fractional heat conduction in porous medium with the generalized Cattaneo model. Appl. Math. Model. **100**, 107–124 (2021)
41. Nikan, O., Avazzadeh, Z.: Numerical simulation of fractional evolution model arising in viscoelastic mechanics. Appl. Numer. Math. **169**, 303–320 (2021)
42. Nikan, O., Avazzadeh, Z., Machado, J.: Numerical study of the nonlinear anomalous reaction–subdiffusion process arising in the electroanalytical chemistry. J. Comput. Sci. **53**, 101394 (2021)
43. Nikan, O., Avazzadeh, Z., Machado, J.T.: Numerical approximation of the nonlinear time-fractional telegraph equation arising in neutron transport. Commun. Nonlinear Sci. Numer. Simul. **99**, 105755 (2021)
44. Rasoulizadeh, M., Nikan, O., Avazzadeh, Z.: The impact of LRBF-FD on the solutions of the nonlinear regularized long wave equation. Math. Sci. **15**, 365–376 (2021)
45. Nikan, O., Avazzadeh, Z., Machado, J.T.: Numerical investigation of fractional nonlinear sine-Gordon and Klein-Gordon models arising in relativistic quantum mechanics. Eng. Anal. Bound. Elem. **120**, 223–237 (2020)
46. Wendland, H.: Scattered Data Approximation, vol. 17. Cambridge University Press, Cambridge (2004)
47. Shepard, D.: A two-dimensional interpolation function for irregularly-spaced data. In: Proceedings of the 1968 23rd ACM National Conference, pp. 517–524 (1968)
48. Wendland, H.: Piecewise polynomial, positive definite and compactly supported radial functions of minimal degree. Adv. Comput. Math. **4**(1), 389–396 (1995)